PLASTIC DEFORMATION AND HARDENING CHARACTERISTICS IN THREE-DIMENSIONAL FRACTURE SPECIMENS

E. Thomas Moyer, Jr. and H. Liebowitz

School of Engineering and Applied Science
The George Washington University Washington, D.C. 20052

ABSTRACT

The formulation for general three-dimensional small strain plasticity analysis is presented. A finite element computer code has been developed to carry out the analysis. General hardening characteristics are included as an input option to the program allowing for the study of a wide class of materials.

An example through crack problem is solved employing three different hardening assumptions (isotropic, kinematic and mixed). The plastic deformation in the region of the crack front predicted with each of the models is compared. While the predicted results are similar, several fundamental characteristics of each assumption can be observed. Residual deformation zones are also calculated as a measure of the extent of plastic deformation. The qualitative differences between hardening assumptions are consistent between the plasticity measures allowing for direct comparison with experimental observation.

INTRODUCTION

The study of ductile fracture processes has been widely discussed in the literature during the past decade. Theoretical, numerical, experimental and many combined studies have been presented. Fracture criteria have been proposed based on many controlling quantities (e.g., stress, strain, energy, displacements, etc.) both on global and local scale levels. Without exception, all of these criteria show a marked thickness and geometry dependence limiting their predictive capabilities. While some of the proposed criteria have been successful at predicting certain fracture phenomena for mildly ductile specimens, the geometry dependence of the controlling parameters makes application of these theories to practical specimens extremely difficult. The purpose of this study is to investigate the nature of the plastic deformation near a three-dimensional stationary crack front in a ductile material. Due to the three-dimensional nature of ductile fracture, it is essential to accurately model the stress-strain response for a general three-dimensional crack problem.

The majority of the studies on the plastic deformation near a crack are based on two-dimensional approximations. While these studies are a necessary first step in the study of ductile phenomena, several fundamental effects remain inadequately modeled. For specimens thick enough to be modeled by plane-strain, ductility effects are usually not

significant. Most engineering metals exhibiting significar plasticity effects are relatively thin. It is tempting, therefore, for many applications, to employ a plane-stress analysis. While the gross specimen behavior may be reasonably predicted with such an approach, the local effects near the crack will not be adequately modeled. For linear elastic materials it can be shown that the stress-strain state near a crack front in three-dimensions is essentially plane-strain except at the intersection of the crack with a free surface [1]. For problems involving plasticity, the incremental deformations during loading will exhibit the same characteristic behavior as an elastic body with an elastic modulus equal to the instantaneous tangent modulus [2]. The local, instantaneous response near an arbitrary crack front should be one of plane-strain independent of the specimen thickness. A fully three-dimensional analysis must be employed, therefore, to accurately model the local plastic response of a cracked medium.

To examine the local deformation response of a three-dimensional elastic-plastic crack specimen, a finite element code was developed. The formulation employs an incremental J_2 flow theory of plasticity with an arbitrary, "Mixed" hardening response. Two-dimensional studies have shown that different materials exhibit different hardening properties that can be load and geometry dependent. The generality of the hardening law employed allows for user determined hardening input. The

initial code generated for this study assumes infinitesimal displacements and strains. The formulation is easily modified, however, to account for finite strain effects. This will be the topic of a later study.

The program was tested on many problems of uniform expansion and simple geometric configurations with analytic (or quasi-analytic) solutions. These test runs facilitated the debugging of the convergence algorithms and iterative routines. The present study focuses on a center-cracked sheet made of an aluminum alloy similar in nature to 7075-T6751 aluminum. The response assuming kinematic hardening, isotropic hardening and a combined law is found. The results demonstrate that the local yield effects are moderately sensitive to the hardening law. For the range studied, however, there is not significant enough differences between the models to distinguish a preferred approach. Since reverse yield and cyclic loading have not been investigated, large distinction between hardening models is not anticipated. The similarity of the predicted results, however, serves as a strong indication of the numerical consistency of the solutions.

A comparison was made between the yield zones on the free surface predicted at maximum load with the von Mises stress yield criterion and the residual contractions predicted after unloading. Good correlation was obtained in that the yield characteristics predicted by both measures were

qualitatively similar. The predicted zones using the stress at maximum load were larger than the residual contraction zones as was expected. A contraction of 1.E-04 inches was the smallest contour plotted as this is on the order of resolution of both experimental techniques and the numerical results. While numerical correlations are purely qualitative without experimental calibration, they do serve to demonstrate the consistency and probable accuracy of the code and the mesh employed.

A companion experimental study is currently underway to compare the predicted yield characteristics with the experimentally observed deformations. The difficulty in any such study is the necessity of achieving significant plastic deformation without slow crack growth. The phenomena of slow crack growth is an effect which must be modeled independent of the deformation response. While slow growth is undoubtedly controlled by the local deformation state, the process is a fundamentally different physical failure mechanism. The validity of the plasticity model being employed must be ascertained independent of the fracture characteristics of the specimen.

CONTINUUM PLASTICITY FORMULATION

The goal of continuum plasticity theories is to provide a relationship between the incremental changes in deformation and stress as a material undergoes irreversible deformation. Due to the complex nature of the deformation fields generally produced in a solid, most mathematical theories attempt to extrapolate the phenomena observed in uniaxial tensile tests to more complex stress states. While many such formulations have been advanced, few provide constitutive relations which are practical for analysis of complex structures. Confining the discussion to incremental plasticity theories which are strain rate independent, essentially all the theories currently employed differ only in the hardening assumptions made and the choice of a yield criteria. The two most widely accepted yield criteria are the von Mises (J_2) criteria and the Tresca criteria. The Tresca criteria is mathematically simpler to employ, however, the yield surface exhibits singular points which are undesirable numerically. While these points can be handled with Lagrange multipliers [3], this approach renders the analysis as complex as the von Mises criteria. For most engineering fracture problems, it is generally agreed that the von Mises criteria more accurately models a wider class of materials in more practical applications than the Tresca criterion [4,5].

The incremental theory of plasticity employed in this

work is based on the classical rate proportionality assumptions and J_2 flow theory. While the mathematical details vary with the choice of yield criteria, the salient features of all incremental theories are the same. This discussion will, therefore, be confined to the specific theory employed in this work.

Assuming stress-strain rate proportionality and J_2 flow theory (which assumes the plastic deformations are incompressible) the stress-strain rate relations can be written as [6]

$$\dot{e}_{ij} = \begin{cases} \frac{1+\nu}{E}\dot{S}_{ij} + \frac{3}{2} f(\sigma_e) S'_{ij}\dot{\sigma}_e & \sigma_e = \sigma_y;\ \dot{\sigma}_e > 0 \\ \frac{1+\nu}{E}\dot{S}_{ij} & \text{Otherwise} \end{cases} \tag{1}$$

where:

$\dot{e}_{ij} = \dot{\varepsilon}_{ij} - \frac{1}{3}\dot{\varepsilon}_{pp}\delta_{ij}$ are the deviatoric strain rate components,

ν is Poisson's ratio,

E is Young's modulus,

$S_{ij} = \sigma_{ij} - \frac{1}{3}\sigma_{pp}\delta_{ij}$ are the deviatoric stress components,

a_{ij} are the coordinates in stress space of the yield surface center,

$S'_{ij} = S_{ij} - a_{ij}$ are the deviatoric stress components measured relative to the current yield center,

$\sigma_e = \sqrt{\frac{3}{2} S_{ij}S_{ij}}$ is the effective stress,

$\sigma'_e = \sqrt{\frac{3}{2} S'_{ij}S'_{ij}}$ is the effective stress relative to the current yield center,

σ_y is the current yield stress, and

$\cdot$ denotes time differentiation.

Due to the incompressibility condition, the hydrostatic strain rate is proportional to the mean stress rate and is given by

$$\dot{\varepsilon}_{pp} = \frac{1-2\nu}{E}\dot{\sigma}_{pp} \tag{2}$$

The function $f(\sigma_e)$ is dependent on the uniaxial stress-strain curve and will be discussed subsequently. For a von Mises (J_2) material, the center of the yield surface moves at a rate proportional to the projection of the stress rate vector onto the local normal to the current yield surface and can be written as

$$a_{ij} = \begin{cases} \frac{3}{2}(1 - \beta)\, S'_{k\ell}\dot{S}_{k\ell}S'_{ij}/\sigma'^{2}_{e} & \sigma_e = \sigma_y;\ \dot{\sigma}_e > 0 \\ 0 & \text{Otherwise} \end{cases} \tag{3}$$

where β varying from 0 to 1 will model hardening behavior from kinematic ($\beta = 0$) to isotropic ($\beta = 1$).

The function $f(\sigma_e)$ is derived from the uniaxial stress-strain curve. For an uniaxial specimen, equation (1) reduces to

$$\frac{3}{2}(\dot{\varepsilon}_{axial} - \dot{\varepsilon}_{transverse}) = \frac{2}{3}\frac{(1+\nu)}{E}\dot{\sigma}_e + f(\sigma_e)\,\sigma_e\dot{\sigma}_e \tag{4}$$

in the plastic range. Thus,

$$f(\sigma_e) = \frac{2}{3}(\dot{\varepsilon}_{axial} - \dot{\varepsilon}_{transverse})/\sigma_e\dot{\sigma}_e \tag{5}$$

Invoking incompressibility (i.e., $\dot{\varepsilon}_{transverse} = -\frac{1}{2}\dot{\varepsilon}_{axial}$), the function $f(\sigma_e)$ can be written as

$$f(\sigma_e) = \dot{\varepsilon}_{plastic}/\sigma_e\dot{\sigma}_e \tag{6}$$

If the uniaxial stress-strain curve is expressed in a multi-linear fashion as shown in Figure 1, the stress-strain relation is

$$\varepsilon = \frac{\sigma}{E} + \frac{\alpha_1}{E}(\sigma_1 - \sigma_y) + \frac{\alpha_2}{E}(\sigma_2 - \sigma_y) + \ldots + \frac{\alpha_m}{E}(\sigma - \sigma_m) \tag{7}$$

where $\sigma_{m-1} < \sigma < \sigma_m$ and α_m is given by

$$\alpha_m = \frac{E\Delta\varepsilon_m - \Delta\sigma_m}{\Delta\sigma_m} \tag{8}$$

From equation (7), the plastic strain rate is given by

$$\dot{\varepsilon}_{plastic} = \frac{\alpha_m\dot{\sigma}_e}{E} \tag{9}$$

and thus from (6)

$$f(\sigma_e) = \frac{\alpha_m}{E\sigma_e} \tag{10}$$

Equations (1), (2), (3) and (10) provide a complete set of elastic-plastic constitutive relations. Together with the equilibrium equations and the strain-displacement relations, a governing system will be formed. It is important to note that the constitutive formulation outlined above is acceptable for finite as well as infinitesimal strains. Also of importance is the fact that this formulation is strain-rate independent. This assumption appears to be realistic for most engineering metals at room temperature (or cooler). For high temperature problems a rate-independent formulation is dubious.

FINITE ELEMENT STRESS ANALYSIS

Equations (1), (2), (3) and (10) provide the fundamental relationships between stress and strain rates. The equilibrium conditions (governing equations) for a continuum body in the absence of body forces and inertia effects can be written as

$$\partial \dot{\sigma}_{ij}/\partial x_j = 0 \tag{11}$$

with the boundary conditions

$$\dot{\sigma}_{ij} n_j = \dot{T}_i \text{ on } S_T$$

and (12)

$$\dot{u}_i = \mathring{u}_i \text{ on } S_u$$

where $\dot{T}_i$ are the specified loading rates on the boundary experiencing applied tractions (S_T) and $\mathring{u}_i$ are the velocities specified on the remainder of the boundary (S_u). Utilizing the standard strain-displacement relations*

$$\epsilon_{ij} = \frac{1}{2}(\partial u_i/\partial x_j + \partial u_j/\partial x_i) \tag{13}$$

*The details of the analysis will be limited to infinitesimal strains for mathematical simplicity. The solution procedure with finite strains is identical, however, the notational complexities are considerable.

and either employing the Principle of Virtual Work for increments of displacement or by performing the standard Galerkin technique on the governing equations, (11) and (12), the finite element equations governing the nodal velocities, $\dot{\underset{\sim}{U}}$, can be written in terms of the loading rate vector, $\dot{\underset{\sim}{R}}$, in the form

$$\underset{\sim}{K}(\underset{\sim}{U}) \cdot \dot{\underset{\sim}{U}} - \dot{\underset{\sim}{R}} = 0 \tag{14}$$

The standard finite element assumptions made are given by

$$\underset{\sim}{u} = \underset{\sim}{N} \cdot \underset{\sim}{U}$$

$$\dot{\underset{\sim}{\epsilon}} = \underset{\sim}{B} \cdot \underset{\sim}{U} \tag{15}$$

$$\dot{\underset{\sim}{\sigma}} = \underset{\sim}{D}(\underset{\sim}{U}) \cdot \dot{\underset{\sim}{\epsilon}}$$

$$\underset{\sim}{K}(\underset{\sim}{U}) = \sum_{\text{elements}} \int_{\text{element area}} \underset{\sim}{B}^T \underset{\sim}{D}(\underset{\sim}{U}) \underset{\sim}{B} \, dA$$

where $\underset{\sim}{N}$ are the shape functions and two dimensional analysis has been assumed (as implied by the area integral). The set of rate equations (14) will be integrated one load increment ($\Delta \underset{\sim}{R}$) at a given time to determine the corresponding new displacement increment, $\Delta \underset{\sim}{U}$. The Newton-Raphson or tangent stiffness solution procedure is employed. At load increment L + 1, the initial solution $\Delta \underset{\sim}{U}^i_{L+1}$ is found from

$$\underset{\sim}{K}(\underset{\sim}{U}_L) \cdot \Delta\underset{\sim}{U}^i_{L+1} = \Delta\underset{\sim}{R}_{L+1} \tag{16}$$

The "new" displacement is then used in the stiffness matrix, $K(U_L + \sum_{i=1}^{m} \Delta U^i_{L+1})$, and a new correction is obtained from

$$\underset{\sim}{K}\left[\underset{\sim}{U}_L + \sum_{i=1}^{m} \Delta\underset{\sim}{U}^i_{L+1}\right] \cdot \Delta\underset{\sim}{U}^{m+1}_{L+1} = \Delta\underset{\sim}{R}_{L+1} -$$

$$\int_{U_L}^{U_L + \sum_{i=1}^{m} \Delta U^i_{L+1}} \underset{\sim}{K}(\underset{\sim}{U}) \, d\underset{\sim}{U} = \underset{\sim}{F}^{i+1}_{L+1} \tag{17}$$

where the integral is approximated using Simpson's rule. The procedure is repeated until two convergence criteria are met:

$$\left|\underset{\sim}{F}^{i+1}_{L+1}\right|^2 / \left|\Delta\underset{\sim}{R}_{L+1}\right|^2 \leq C_1$$

and (18)

$$\left|\underset{\sim}{F}^{i+1}_{L+1}\right|^2 / \left|\underset{\sim}{R}_{L+1}\right|^2 \leq C_2$$

where $\underset{\sim}{R}_{L+1}$ is the total load at step L + 1.

In this study, 20-node quadratic isoparametric elements were employed exclusively. All integration was carried out utilizing 3 x 3 x 3 Gauss-Legendre quadrature formulae. Strains were calculated at the Gauss integration points in each element from the strain-displacement relations of (13). Stresses were cumulatively calculated at the Gauss points from the stress-strain relations.

Directly calculating strains and stresses from the finite element relations (15) at points on element boundaries inherently yields poor results. This is especially true when C^0 shape functions are employed. A superior approach is to calculate the stresses and strains at the Legendre quadrature points and to extrapolate or smooth them to the boundaries. This approach has been shown to yield very accurate results for a wide variety of geometric mappings. In this study the smoothing technique as developed in [7] is employed for all stress and strain evaluations.

Currently, four methods of accounting for the crack tip singularity are widely employed. Each of these methods is based on an established technique in LEFM (Linear Elastic Fracture Mechanics). The first method, the enriched element approach (where the shape functions are modified with the asymptotic crack solution vanishing at the nodes) has been employed both for the multilinear stress-strain models and for power law hardening models [8]. Enriched elements based on the power law hardening model assume that the enriched

element is fully yielded. This assumption is physically unrealistic, especially behind the crack tip. The singular solution employed for the power law hardening case also assumes a circular yield zone which is far from realistic. The solutions generated using enriched elements and a multilinear stress-strain assumption are reasonably accurate providing a judicious choice of enriched element size and surrounding grid characteristics is made. The major drawback to the use of enriched elements is the computation time required to obtain convergence due to element incompatibility. The second method, the most basic approach, uses a very fine mesh near the crack tip and employs only conventional elements. This method produces reasonable results far from the crack region but questionable local results. Convergence is usually rapid, therefore, gross specimen behavior can be obtained quickly. With unrealistically fine grids, good local results can be obtained (except in the elements bordering the crack tip) but only at the expense of computer time [9]. The third method is based on the fact that if isoparametric elements are chosen with midside nodes, judicious choice of the placement of these nodes results in the inducement of a $\sqrt{r}$ term in the displacement shape functions [10, 11]. These elements are essentially equivalent to enriching the shape functions, however, element compatibility is preserved resulting in faster convergence. The fourth technique of modeling crack tip behavior is through the use of hybrid elements where elements bordering a surface

with traction boundary conditions are forced to satisfy those conditions exactly and the elements bordering a surface with displacement boundary conditions are also forced exactly. The element boundaries are then matched by using Lagrange multipliers in the variational equations to ensure element equilibrium and continuity in an approximate sense. Little work has been done on comparisons of hybrid methods to conventional methods in elastic-plastic crack problems, however, the technique was applied with questionable success in [12]. The preferred method in the literature is still to use a very fine mesh and standard elements. Complete discussions of the above methods can be found in [13-15].

In this study, only conventional 20-node elements are employed. Studies on linear elastic through-crack specimens has demonstrated the accuracy of this approach for predicting local stress responses. Since the details of the local singularity are unknown in the plasticity case, this approach is the most likely to delineate the characteristics of the numerical solution without the influence of singularity assumptions. The grid employed is shown in Figures 4a, 4b and 4c. The accuracy of the results predicted by this grid are discussed in [16] for the linear elastic case. The choice of grid characteristics is based on the convergence study cited above. Since there are no known three-dimensional elastic-plastic bench mark solutions available for comparison, linear convergence studies appear to be the most reliable

indicator of mesh accuracy. Few numerical solutions have been presented in the literature for three-dimensional elastic-plastic crack problems. The studies that have been done have been limited to initial stress approaches (e.g., [17]) or deformation theory approaches (e.g., [18]). These were severely limited in grid density due to computational restrictions, therefore, no comparison has been attempted. The computational requirements of the present approach are extreme and will be discussed subsequently.

PROBLEM DESCRIPTION AND FINITE ELEMENT MODELING

The problem chosen for study is that of a center-cracked plate with a through crack. The plate has dimensions of 7 inches in length, 3.5 inches in width with a thickness of .5 inches. The applied load is assumed to be normal to the crack orientation as shown in Figure 2 (i.e., Mode I loading). The material properties chosen are typical of many aluminum alloys. The assumed elastic properties are

$$E = 10.5\ E + 06\ PSI$$

$$\nu = 0.3$$

$$\sigma_y = 59.00\ E + 03\ PSI$$

The uniaxial stress-strain curve models the behavior of 7075-T7651 aluminum. A trilinear approximation is employed in the analysis. Both a typical experimental curve and the trilinear approximation are shown in Figure 3. The effect of hardening behavior modeling is studied by varying the hardening parameter β, defined in equation (3). Isotropic hardening ($\beta = 0$), kinematic hardening ($\beta = 1$) and a mixed state ($\beta = 0.5$) were modeled.

The finite element grid employed consists of 96 20-node isoparametric elements with quadratic shape functions. No "singular" elements are employed due to the unknown nature of the crack front singularity in plasticity. The grid is shown in Figures 4a, 4b and 4c. Computationally this grid is

extremely expensive. The convergence studies cited previously have demonstrated the advantages and desirability of this approach. The grid has 1872 total degrees of freedom and requires approximately 1 hour and 13 minutes of CPU time on a VAX-11/780 to complete each iteration. Where significant plasticity occurred, extreme runtimes where required (often on the order of several days). While the current approach is believed to be very accurate and reproducing the necessary resolution to accurately describe the three-dimensional elastic-plastic crack phenomena, the complexity of the calculation and extreme computational requirements should be appreciated at the outset. Three-dimensional elastic studies have indicated that these computational requirements are necessary for accurate solution [7]. It is dubious that simpler approaches will be able to predict the local fields with any degree of confidence.

RESULTS AND DISCUSSION

The yield zones predicted at the maximum load for each of the three hardening models were calculated and plotted both on the free surface and on the midplane. The stress components were calculated in each element at the quadrature points and interpolated to the surfaces using the technique discussed previously.

Figure 5 is a plot of the von Mises stress contours predicted on the free surface at the maximum load assuming an isotropic hardening law. The maximum plastic radius predicted is 0.541 inches. The extent of the plastic zone ahead of the crack tip is 0.169 inches, predicting a fairly rotund zone. Figure 6 is a plot of the von Mises stress contours predicted on the free surface with a kinematic hardening model. The maximum plastic radius of 0.524 inches and crack line extent of 0.148 inches are both significantly less than predicted with isotropic hardening. The results assuming a mixed hardening model are shown in Figure 7. The maximum plastic radius of 0.544 inches is almost identical to the isotropic model. The crack line extent predicted, however, is much less than those predicted with either a kinematic or isotropic model. The predicted zone is much narrower than the other models demonstrate. It is unknown whether this phenomena is due to the inaccuracies of the numerical results or the physical assumptions. The narrower predicted yield zone is consistent

with the dilatant stress field anticipated in front of the crack.

Figure 8 is a plot of the von Mises contours predicted on the midplane at the maximum load with an isotropic hardening model. As expected, the zone is smaller than the surface zone. The yielding along the crack line is, however, almost identical to the surface prediction. Figures 9 and 10 show the predicted midplane zones for the kinematic and mixed hardening assumptions In both cases, the yielding extent ahead of the crack tip is very close to that predicted on the surface. The differences between the maximum radii of the predicted midplane zones are less than the surface zones. This phenomena is consistent with the smaller amount of plasticity and the nearly plane-strain conditions on the midplane.

One approach to predicting the extent of plastic deformation is to measure or calculate the amount of surface contraction or residual deformation on the surface after the specimen has been unloaded. Inside the plastic region measurable residual deformation should exist. Figure 11 is a plot of the surface contraction predicted after the specimen was unloaded to zero applied load assuming a kinematic hardening model. Contraction contours of 1.E-04 inches to 5.E-04 inches are shown. The lowest contour plotted (1.E-04 inches) is on the order of the deformation resolvable in the laboratory and is also on the anticipated accuracy of the finite element method being employed. The predicted plastic region is smaller than

that predicted by the von Mises stress measure discussed above (Figure 6). This is not unexpected as the stress criterion is more sensitive to minimal plastic deformation. The yielded extent predicted ahead of the crack tip is larger, however, than predicted above. The deviation from a dilatational stress state ahead of the tip will be detected sooner by the residual deformation than by the effective stress (a large deviatoric stress field must be present to create a von Mises stress larger than the yield stress whereas any deviation in the neighborhood of a significant residual field will cause surface contractions). Figures 12 and 13 are plots of the surface contours predicted with isotropic and mixed hardening models. Consistent with the von Mises stress predictions, the zones with an isotropic model are larger than those predicted with any of the other models. The mixed hardening model predicts zones which are similar to the isotropic zones with less yielding directly ahead of the crack tip. All three models demonstrate more residual deformation ahead of the tip than would be expected from the stress results.

CONCLUSIONS

The finite element formulation for general three-dimensional elastic-plastic bodies undergoing infinitesimal deformation has been presented. A computer code has been developed and an example crack problem was solved with three widely employed hardening models. The crack front yield zones predicted are very similar in size and shape. For many applications, the differences may be negligible. Significant variation in crack line extent yielding and surface curvature was discovered. It is unknown at present as to which model will more accurately describe different metals of interest to engineers. The predicted differences are so slight, however, that full three-dimensional experimental studies will be needed to discern a valid model for specific applications.

To compare theoretical and experimental predictions, it is proposed to measure the residual deformation on the surface of the specimen in the unloaded state. The theoretical study presented above demonstrates that the finite element predictions are qualitatively realistic and sensitive to hardening characteristics. Comparison with experimental results will delineate the grid characteristics and hardening models which best model specific geometric and material applications. After successful "tuning" of the finite element model, a complete description of the stress and energy state in a cracked body can be predicted with confidence. Once fully three-

dimensional stress fields are predicted, ductile failure theories can be tested and skeptically compared without the bias of unrealistic analytical approximations.

ACKNOWLEDGEMENTS

This work was sponsored by the Office of Naval Research under Contract Number: N00014-75-C-0946.

REFERENCES

[1] G. C. Sih and R. J. Hartranft, "The Use Of Eigen-Function Expansions In The General Solution Of Three-Dimensional Crack Problems," Journal of Mathematics and Mechanics, Vol. 19, No. 2, 1969, pp. 123-138.

[2] S. W. Key, "A Finite Element Procedure For Large Deformation Dynamic Response Of Axisymmetric Solids," Computer Methods In Applied Mechanics And Engineering, Vol. 4, 1974, pp. 195-218.

[3] W. T. Koiter, "Stress-Strain Relations, Uniqueness, And Variational Theorems For Elastic-Plastic Materials With Singular Yield Surface," Quarterly Applied Mathematics, Vol. 11, 1953, pp. 350-354.

[4] P. G. Hodge and G. N. White, "A Quantitative Comparison Of Flow And Deformation Theories Of Plasticity," Journal of Applied Mechanics, Vol. 17, 1950, pp. 180-184.

[5] D. G. H. Latzgo (ed.), Post Yield Fracture, Applied Science, Ltd., New York, 1979.

[6] L. M. Kachanov, Foundations Of The Theory Of Plasticity, North-Holland Publishing Co., 1971.

[7] E. T. Moyer, Jr., "A Brief Note On The 'Local Least Squares' Stress Smoothing Technique," Accepted For Publication in Engineering Fracture Mechanics, 1982.

[8] P. D. Hilton and L. N. Gifford, "Evaluation Of Some Crack Tip Finite Elements For Elastoplastic Fracture Analysis," DTNSRDC Report 79/052, July 1979.

[9] W. K. Wilson and J. O. Osias, "A Comparison Of Finite Element Solutions For An Elastic-Plastic Crack Problem," International Journal Fracture, Vol. 14, 1978, R95-R108.

[10] S. L. Pu and M. A. Hussain, "The Collapsed Cubic Isoparametric Element As A Singular Element For Crack Problems," International Journal Numerical Methods Of Engineering, Vol. 12, 1978, pp. 1727-2742.

[11] S. E. Benzley, "Nonlinear Calculations With A Quadratic Quarter-Point Crack Tip Element," International Journal Fracture, Vol. 12, 1976, pp. 475-477.

[12] S. N. Atluri and K. Katherisan, "3-D Analysis Of Surface Flaws In Thick Walled Reactor Pressure-Vessels Using Displacement-Hybrid Finite Element Method," Nuclear Engineering Design, Vol. 51, 1979, pp. 163-176.

[13] O. C. Zienkiewicz, The Finite Element Method, McGraw-Hill, New York, 1977.

[14] J. T. Oden, Finite Elements Of Nonlinear Continua, McGraw-Hill, New York, 1972.

[15] A. J. Fawkes, D. R. J. Owen and A. R. Luxmoore, "An Assessment Of Crack Tip Singularity Models For Use With Isoparametric Elements," Engineering Fracture Mechanics, Vol. 11, 1979, pp. 143-159.

[16] E. T. Moyer, Jr. and H. Liebowitz, "Comparative Study On Three-Dimensional Crack Tip Modeling Methodology." To be presented at the International Conference on Application Of Fracture Mechanics To Materials And Structures, Freiburg, Germany, June 20-24, 1983.

[17] G. C. Sih and B. V. Kiefer, "Nonlinear Response Of Solids Due To Crack Growth And Plastic Deformation," International Nonlinear And Dynamic Fracture Mechanics, ASME AMD, Vol. 35, 1979, pp. 135-156.

[18] O. C. Zienkiewicz, "Viscoplasticity, Plasticity, Creep, And Viscoplastic Flow." Proceedings of the International Conference On Computational Methods of Nonlinear Mechanics, University of Texas, 1974.

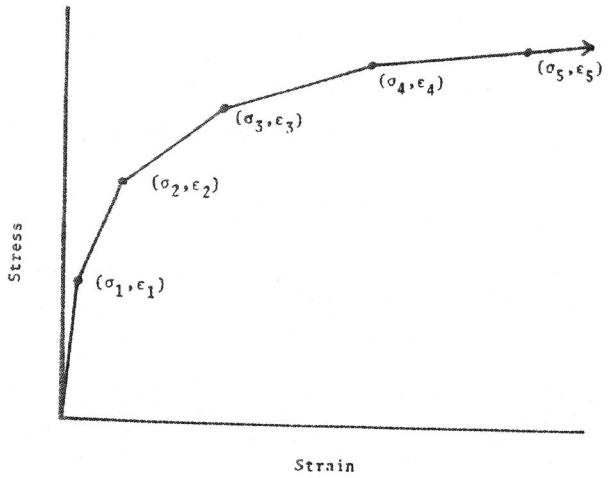

Figure 1: Multilinear Approximation For A Uniaxial Stress-Strain Curve With Hardening.

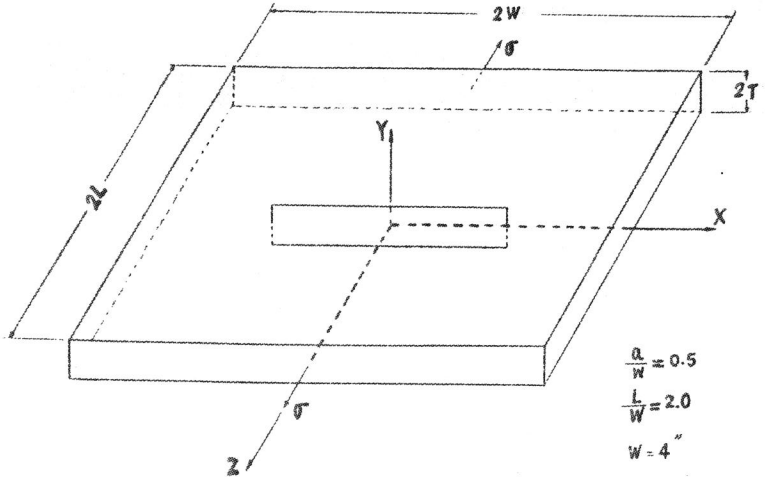

Figure 2: Through Crack Geometry And Loading.

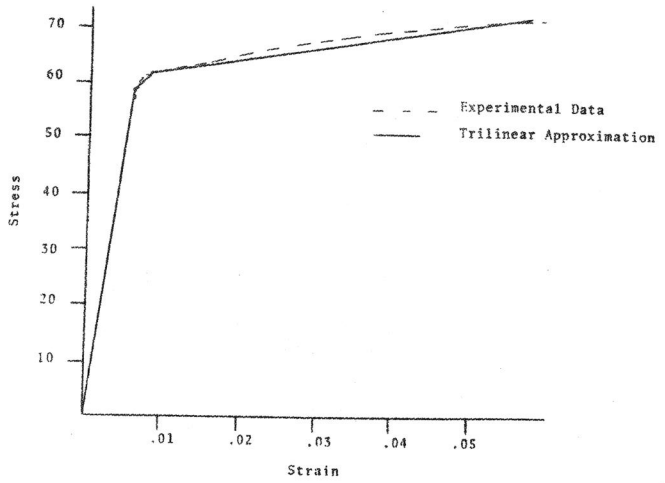

Figure 3: Uniaxial Stress-Strain Curve For 7075-T6751 Aluminum.

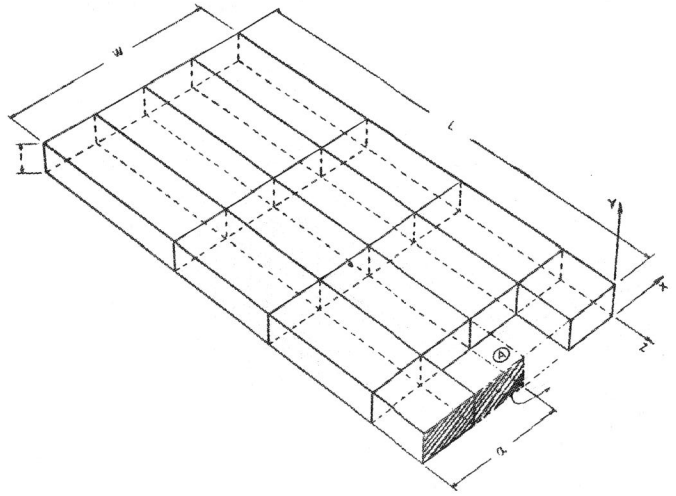

Figure 4a: Finite Element Grid - Coarse Outer Region.

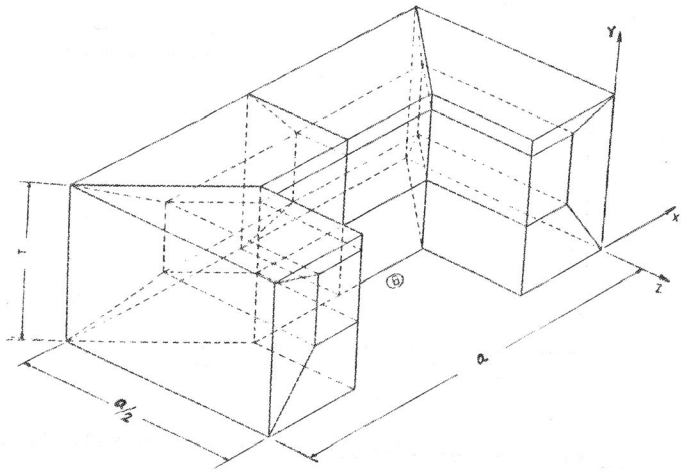

Figure 4b: Finite Element Grid - Blowup Of Region A.

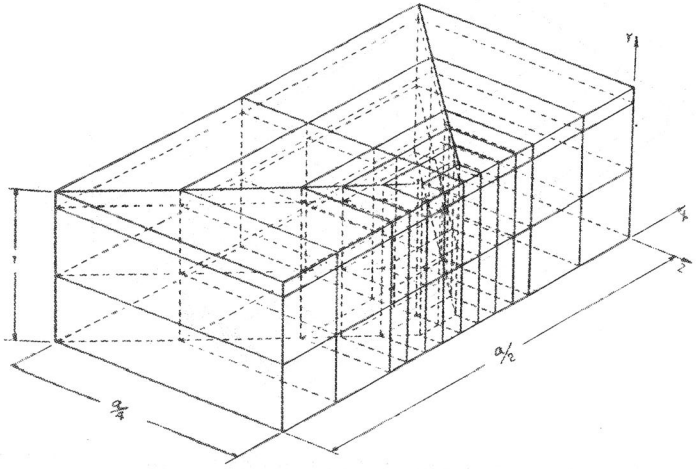

Figure 4c: Finite Element Grid - Near Tip Region B.

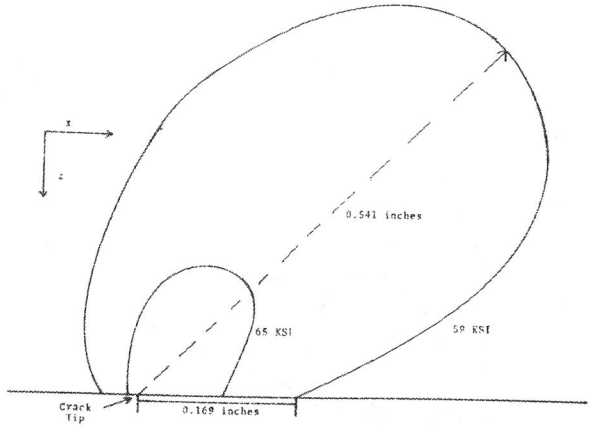

Figure 5: von Mises Stress Contours Near The Crack Tip On Specimen Surface At Maximum Load - Isotropic Hardening.

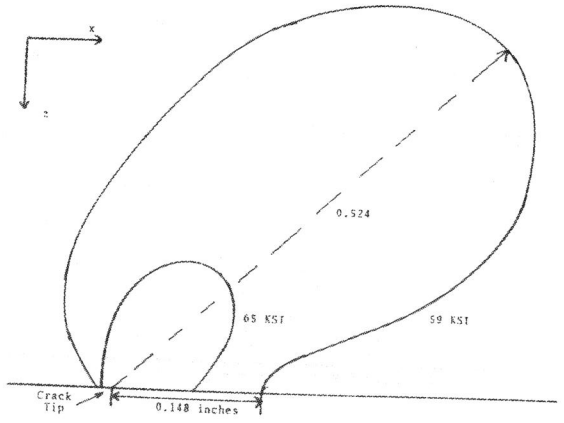

Figure 6: von Mises Stress Contours Near The Crack Tip On Specimen Surface At Maximum Load - Kinematic Hardening.

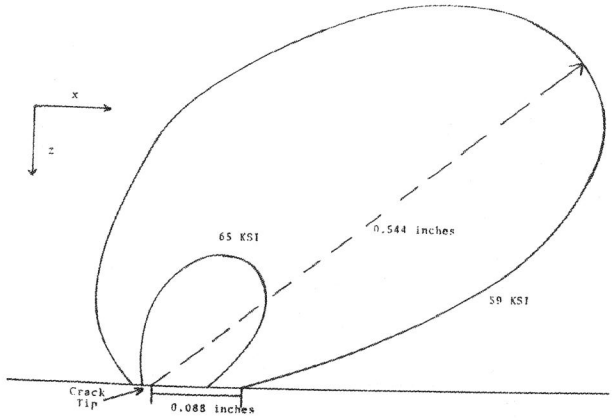

Figure 7: von Mises Stress Contours Near The Crack Tip On Specimen Surface At Maximum Load - Mixed Hardening.

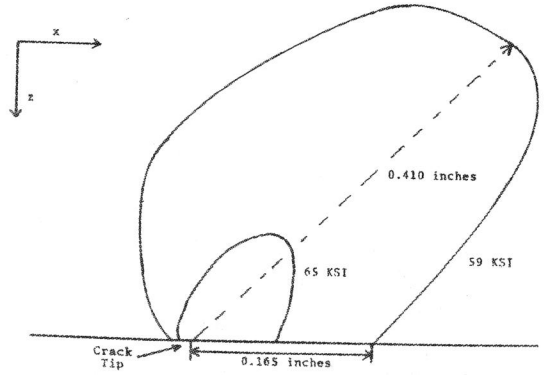

Figure 8: von Mises Stress Contours Near The Crack Tip On Specimen Midplane At Maximum Load - Isotropic Hardening.

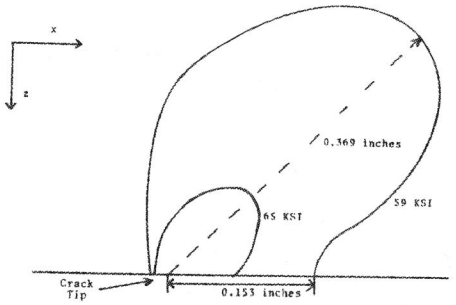

Figure 9: von Mises Stress Contours Near The Crack Tip On Specimen Midplane At Maximum Load Kinematic Hardening.

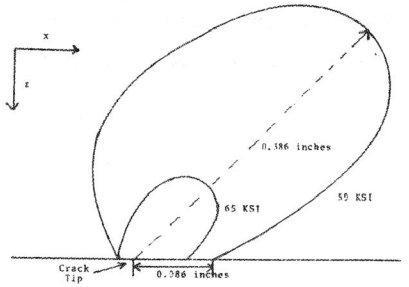

Figure 10: von Mises Stress Contours Near The Crack Tip On Specimen Midplane At Maximum Load - Mixed Hardening.

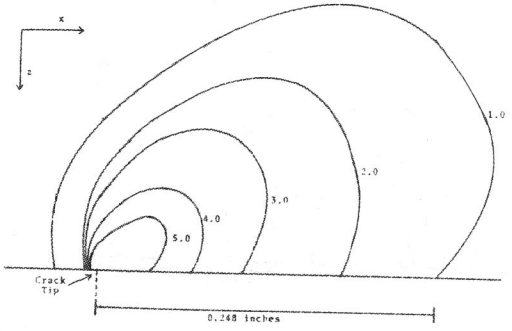

Figure 11: Surface Contractions Near Crack Tip After Unloading - Kinematic Hardening (x 10^{-4} inches).

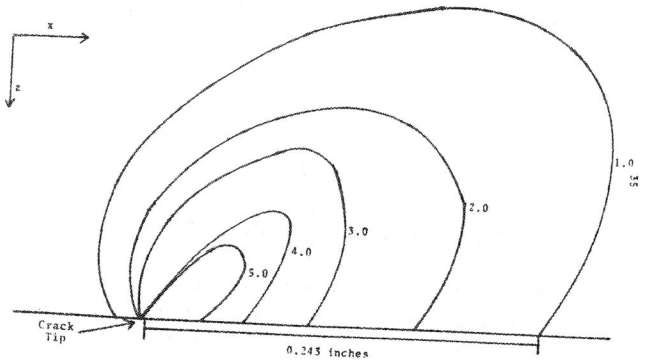

Figure 12: Surface Contractions Near Crack Tip After Unloading - Isotropic Hardening (x 10^{-4} inches).

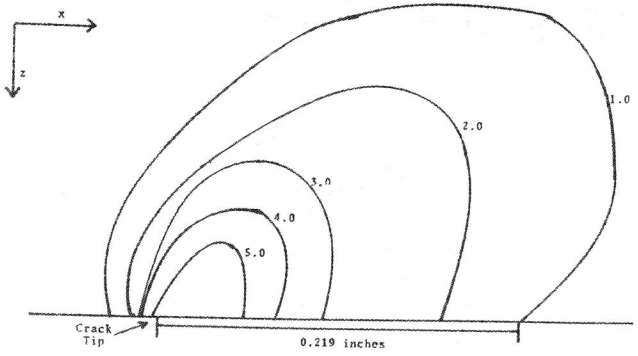

Figure 13: Surface Contractions Near Crack Tip After Unloading - Mixed Hardening (x 10^{-4} inches).